UCID--20755
DE86 011007

THERMAL MANAGEMENT FOR LLNL/UC/SSRL BENDING MAGNET BEAMLINE VIII AT STANFORD SYNCHROTRON RADIATION LABORATORY

Eric J. Berglin
Lawrence Livermore National Laboratory
and
Francis C. Younger
Brobeck Corporation

May, 1986

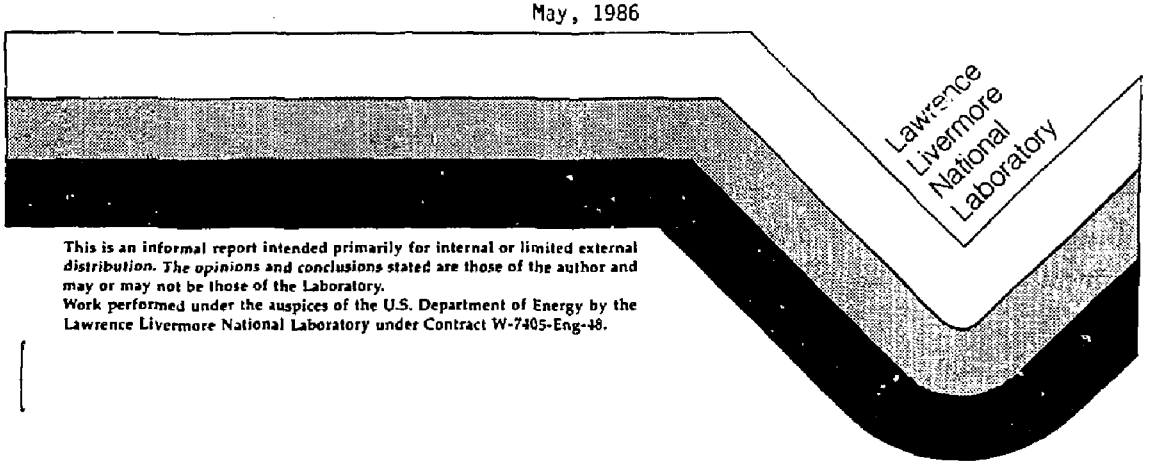

TABLE OF CONTENTS

LIST OF FIGURES

LIST OF TABLES

THERMAL MANAGEMENT FOR LLNL/UC/SSRL BENDING MAGNET FOR BEAMLINE VIII AT STANFORD SYNCHROTRON RADIATION LABORATORY

BY: Eric Berglin, Lawrence Livermore National Laboratory
and
Francis C. Younger, Brobeck Corporation

INTRODUCTION

This report, covering the thermal management for Beamline VIII at SSRL attempts to catalog all the important heat loads on the elements of this beamline. The principal elements are identified and their heat loads tabulated for various loading scenarios. The expected heat loads are those from normal operations including the anticipated performance improvements planned for the SPEAR ring and from abnormal operations due to positional perturbations of the electron beam. The perturbations seen at Beamline VIII will be extremely small when the storage ring is operated in the dedicated mode but may be fairly large for operation in the parasitic mode or for accidental steering errors. When these perturbations are significant, the synchrotron light will be offset slightly from its normal position causing some off-axis rays to strike regions normally shadowed by the beam masks. Thus, some regions which receive little or no heat loading under normal operation, can receive significant heating during abnormal operation.

The layout beam for Beamline VIII is shown in Figure 1. It is divided into two main paths for different experimental purposes in addition to a third path used primarily for beam monitoring. The two main paths are distinguished by the proportional amount of beam assigned to each and by the portion of the energy spectrum they utilize. One path is designated as the VUV line because it utilizes a portion of the spectrum of the vacuum ultraviolet region from 8 eV to 185 eV. The other is the SXR line, which utilizes a portion of the spectrum in the soft x-ray region from 60 to 1100 eV.

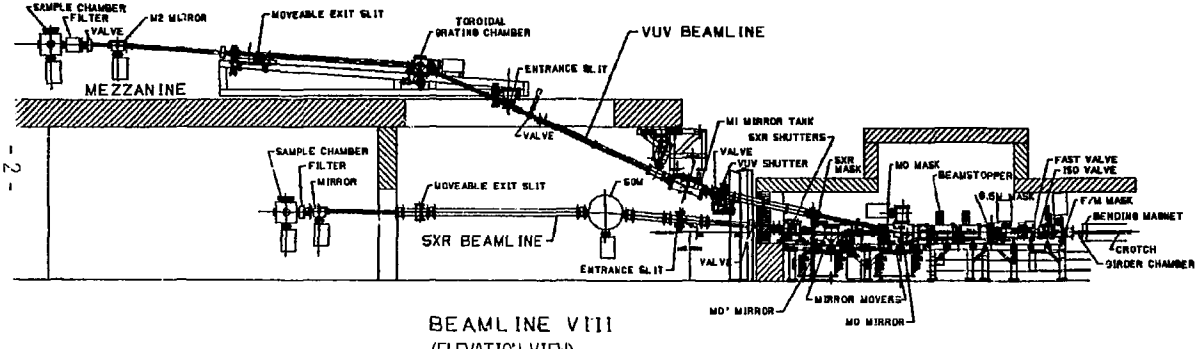

BEAMLINE VIII
(ELEVATION VIEW)

FIGURE 1. BEAMLINE VIII ELEVATION VIEW

SYNCHROTRON RADIATION POWER

The SPEAR storage ring synchrotron radiation that is of concern for Beamline VIII is produced in a bending magnet and comes out along a line tangent to the path which the electrons traverses in the bending magnet. Since the bending magnets in the SPEAR ring bend the electron beam through an angle of about 10°, the radiation comes out in a fan with a horizontal spread of about 10° (175 mr). Beamline VIII will be allocated about 23 mr of this fan, for which 12 mr will be directed to the VUV line and 5 mr will be directed to the SXR line, 0.7 will be used for beam monitoring. The remaining 5.3 mr of the available fan width will be lost as heat on the masks and shields under normal operating conditions. The radiation fan has a fairly large horizontal spread, but a very narrow vertical spread. Most of the beam power will reside within a vertical opening half angle, θ, equal to $1/\gamma$, where γ is equal to the electron total energy divided by its rest energy ($\gamma = E/mc^2$).

The radiation power in the fan from a bending magnet is found from the following equation:(1)

$$Q = 88.47 \times \frac{E^4}{\rho} \times \frac{I}{2\pi} \quad W/mr$$

Where (E) is the electron energy in GeV, ρ is the bending radius of curvature in meters and I is the beam current in amps.

(1) All computations of radiation power and distributions, spectral and spacial, are based on equations from "Properties of Synchrotron Radiation" by Herman Winick. Programs for calculations and plotting results are by the authors. Appendix I gives all calculational methods with appropriate equations.

The radiation covers a wide spectrum of wavelengths. The spectral distribution are shown in Figures 2 and 3 for 3.0 GeV and 3.7 GeV respectively. The critical wavelength and critical energy is found from

$$\lambda_c = 5.59\ \rho/E^3 \text{ and } E_c = .002218\ E^3/\rho$$

Where λ_c is the critical wave length in Angstroms, ρ is the bend radius in meters, E is the electron energy in GeV, and E_c is the critical energy. Half of the integrated power occurs at wavelengths longer than the critical value and half at shorter wavelengths. Figures 4 and 5 show the integrated power. The photon energy at the 50% point is the value corresponding to the critical wavelength.

For the VUV line, the wavelengths for photon energies of interest (8 to 185 eV) are longer than 65 Å. From Figures 4 and 5, it can be seen that less than 2% of the radiated power is in this portion of the spectrum although a large number of low energy photon will be available. For the soft x-ray line with a maximum photon energy of 1100 eV (wavelength = 11.3 Å), the available power at 3.0 GeV is less than 13% of the total power. At 3.7 GeV, the critical wavelength is much shorter and the percent of total power that is available at wavelengths longer than 11.3 Å drop to less than 6% of the total power. Clearly, a large percent of the radiation power is not in the long wavelength portion of the spectrum used experimentally in Beamline VIII and must be dissipated as heat. A large percent of this heat will be dissipated on the masks and first mirrors(2) (M0 and M0').

For the SPEAR storage ring, the magnetic radius is 12.7 meters. The beam energy and current are variables that depend upon the operating conditions. The available RF power to the ring limits the beam energy for a given beam

(2) Detailed calculations of mirror cooling and thermal distortion is covered in "Thermal Loading Considerations for Synchrotron Radiation Mirrors," F.R. Holdener, et al, UCRL-94155, March 1986.

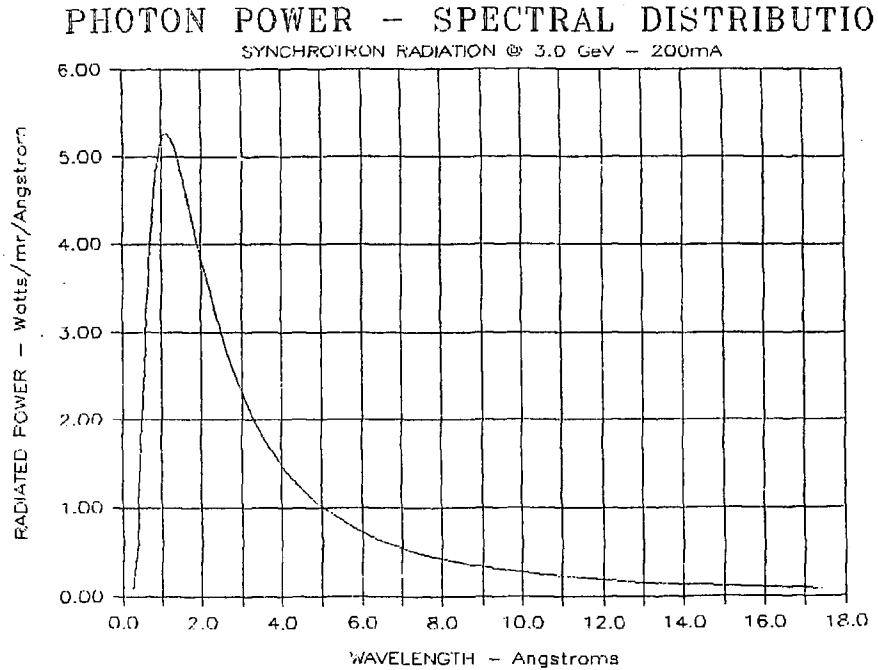

FIGURE 2. RADIATION POWER AS A FUNCTION OF WAVELENGTH FOR SPEAR RING AT 3 GeV AND 200 mA.

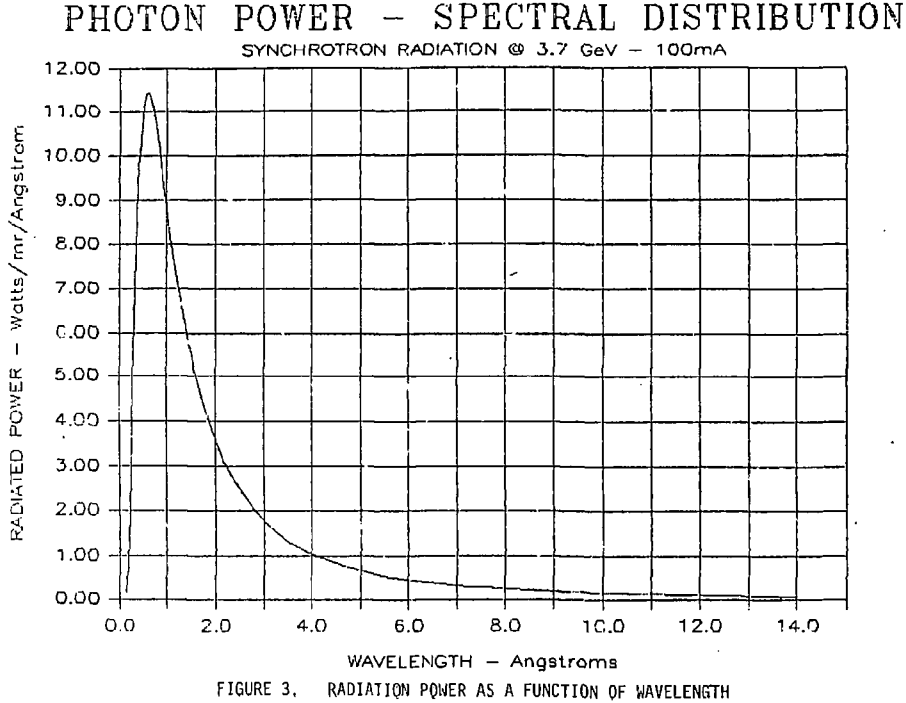

FIGURE 3. RADIATION POWER AS A FUNCTION OF WAVELENGTH FOR SPEAR RING AT 3.7 GeV AND 100 mA.

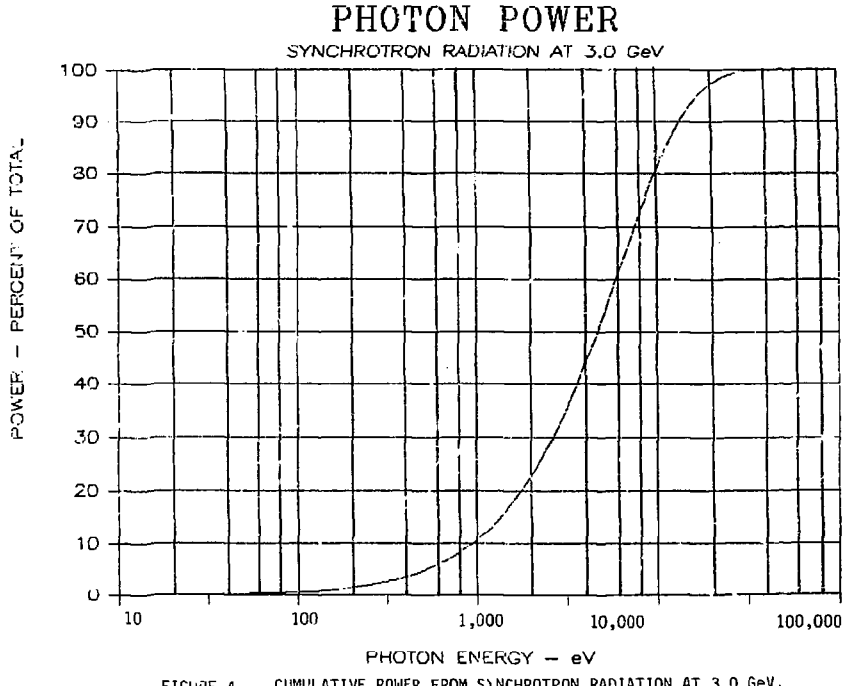

FIGURE 4. CUMULATIVE POWER FROM SYNCHROTRON RADIATION AT 3.0 GeV.

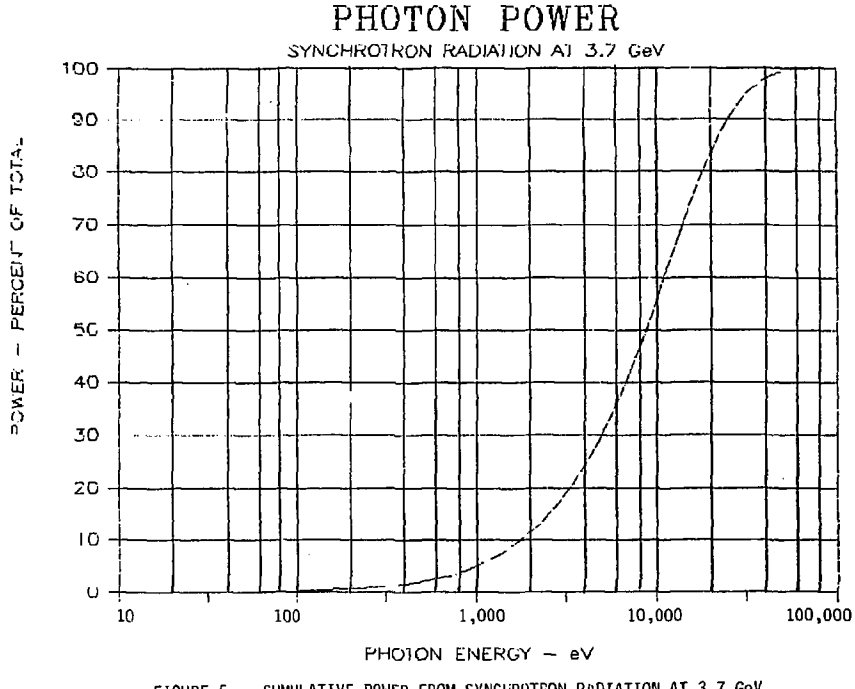

FIGURE 5. CUMULATIVE POWER FROM SYNCHROTRON RADIATION AT 3.7 GeV.

current. For our purposes, two maximum heat load conditions are analyzed. One is for a 3.0 GeV electron beam at a current of 200 mA. The other is for 3.7 GeV at 100 mA. Both of these conditions are for expected future improvement and lead to heat loads more than double that for the present dedicated mode of operations at 3.0 GeV. The total radiation power, half angles, and critical energy are tabulated in Table 1 for both these conditions. The vertical dispersions are illustrated in Figures 6 and 7, which show that the power intensity integrated over all wavelengths is approximately a Gaussian distribution and that about 85% of the total energy lies within the vertical opening angle ($2/\gamma$). It is also clear that about 15% lies outside this angle.

The vertical dispersion shown is dependent upon electron energy and also upon the photon energy. The vertical dispersion is much less for short wavelengths than for long wavelengths. The greater vertical dispersion which occurs at the long wavelengths requires that the VUV beamline have much greater vertical aperture than is needed for the SXR beamline. The vertical dispersions for the VUV and SXR beamlines are shown in Figures 8 and 9 respectively. For the VUV line at the 9.4 eV photon energy shown, 90% of this energy lies within an opening angle of $\pm$ 1.5 mr. At higher photon energy, the angle rapidly decreases. At 94 eV, 90% of the energy is within $\pm$ 0.7 mr. To capture a very large fraction of the photons in the VUV energy range from 8 to 185 eV, a vertical aperture of 3 mr is provided.

For the SXR line, the energy range of interest is from 60 to 1100 eV. For this energy range, a vertical aperture of 1.5 mr permits a very large fraction of the photons to be captured. At 60 eV, for example, about 85% of the photon lie within a vertical angle of $\pm$ 0.75 mr. At 1100 eV, 90% lies

TABLE 1

OPERATING CONDITIONS

CASE	Present Dedicated Operation	With Expected Improvements A	B
Beam Energy, GeV	3.0	3.0	3.7
Beam Current, mA	100	200	100
Photon Power, Watt/mr	8.98	17.96	20.78
Vertical Opening Half Angle $(\frac{1}{\gamma})$, mr	.170	.170	.138
Critical Energy, eV	4719	4719	8852
Critical wavelength, Å	2.627	2.627	1.401

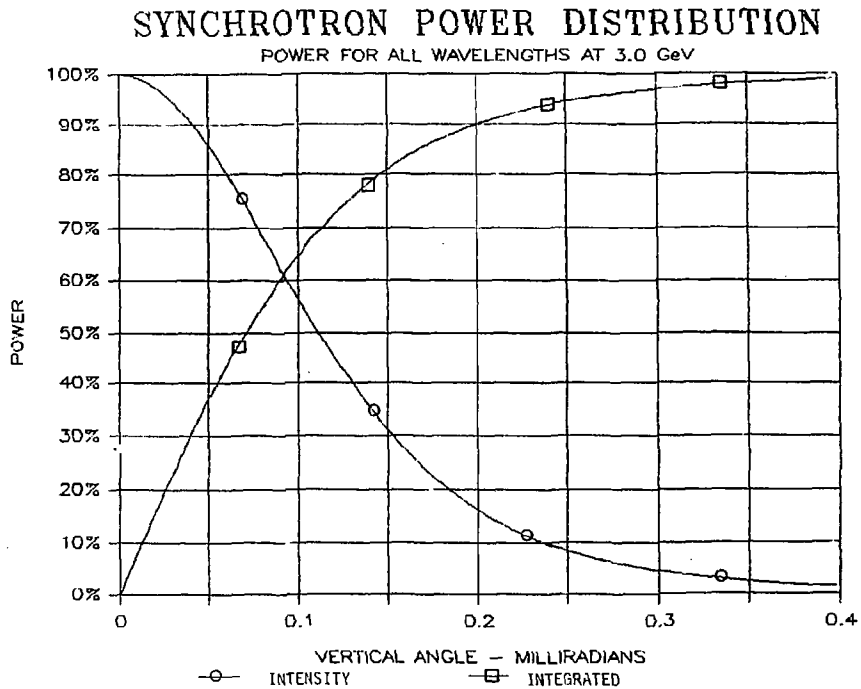

FIGURE 6. VERTICAL DISPERSION OF SYNCHROTRON RADIATION AT 3.0 GeV.

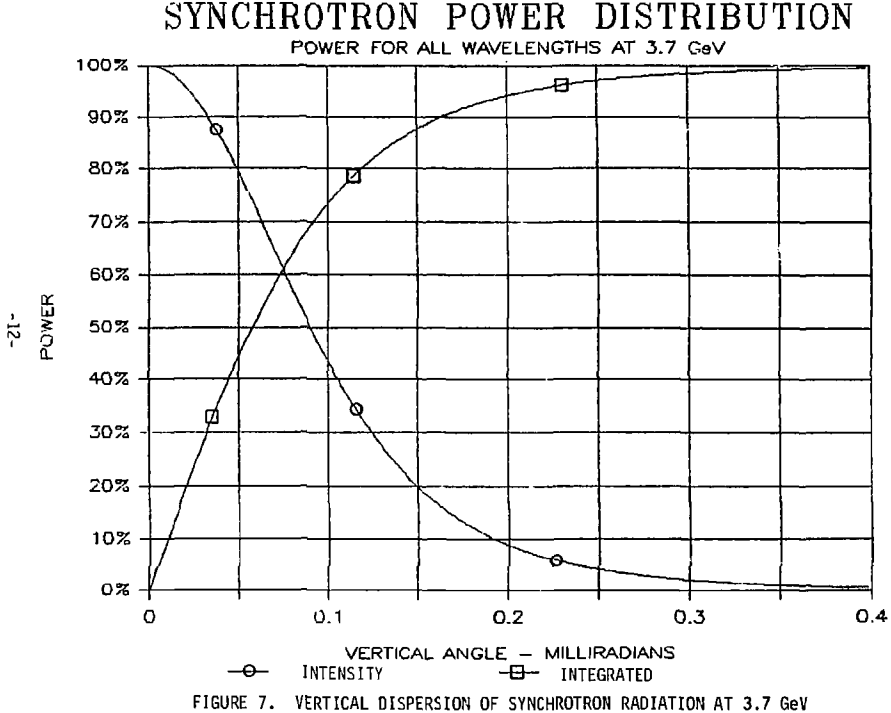

FIGURE 7. VERTICAL DISPERSION OF SYNCHROTRON RADIATION AT 3.7 GeV

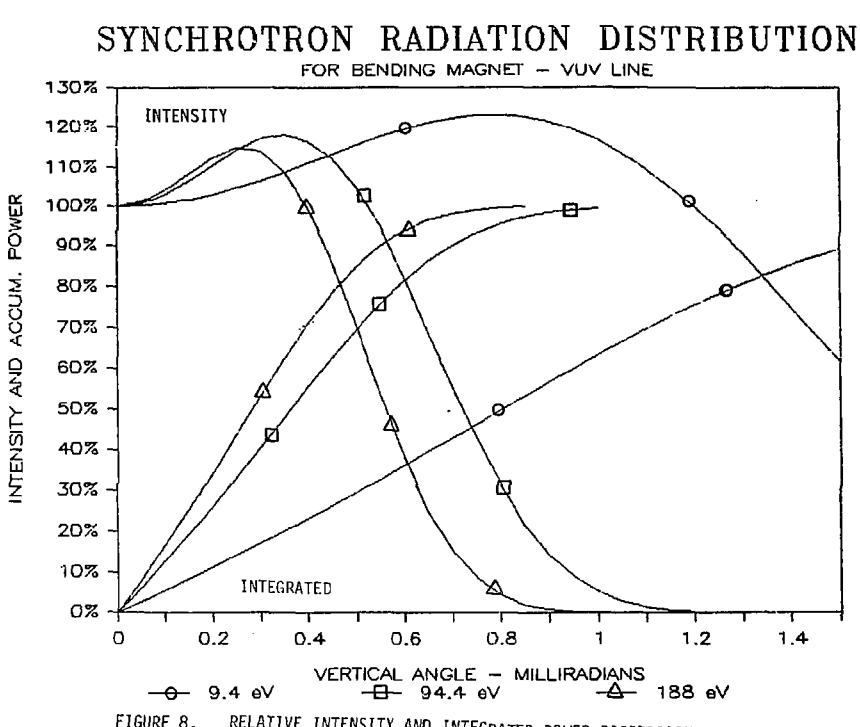

FIGURE 8. RELATIVE INTENSITY AND INTEGRATED POWER DISPERSION AT 3.0 GeV.

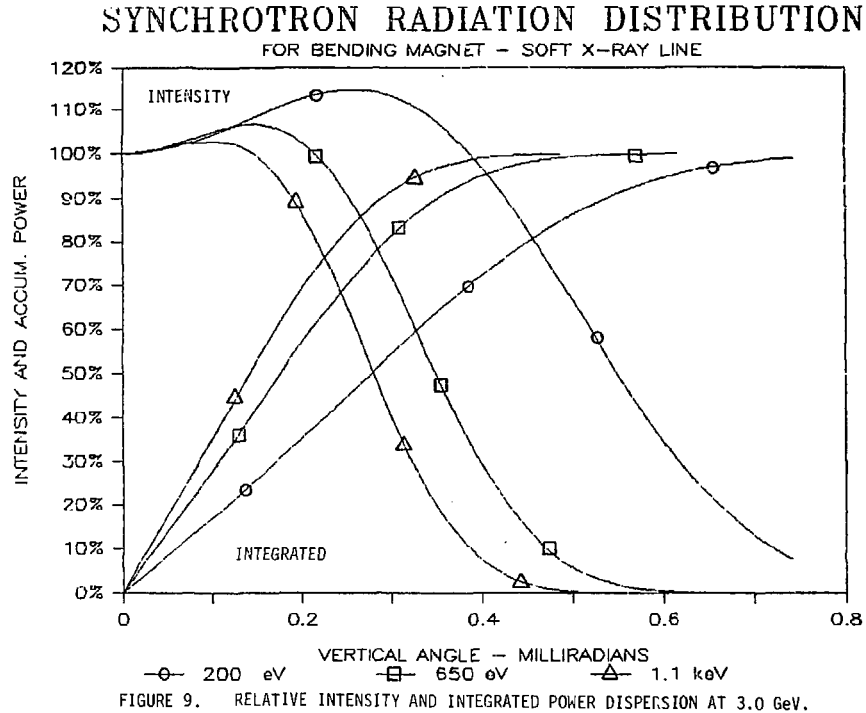

FIGURE 9. RELATIVE INTENSITY AND INTEGRATED POWER DISPERSION AT 3.0 GeV.

within an angle of ± 0.3 mr. A vertical aperture of 1.5 mr is provided for the SXR.

ENERGY DISTRIBUTION

The portion of the synchrotron radiation fan from the bending magnet assigned to Beamline VIII will be allocated to three branches, one for soft x-rays (SXR), another for vacuum ultra-violet (VUV), and the last for the beam position monitor (PM). The nominal allocation of the beam for these paths in terms of horizontal fan angle and vertical divergence is shown in Figure 10. The actual fraction of the photon beam going to each path is controlled by a series of masks and restrictions in the beamline. The effectiveness of these masks and restrictions is to some extent dependent upon the electron energy and the location of the electron orbit in the storage ring.

A particular location of the orbit within the bending magnet is used to define the source point. For various operating scenarios, the electron orbit may deviate slightly from the referenced orbit. Normally, this deviation is very small[3] not exceeding a few millimeters horizontally or vertically. However, for the worst case scenarios, the source may be displaced horizontally by as much as $\pm$ 10 mm and vertically by as much as $\pm$ 6 mm. Moreover, a vertical angular error as great as $\pm$ 0.8 mr may occur. It may be assumed that the combined vertical offset and angle may be represented by an ellipse in vertical phase space. (At the source, the ellipse will have semi-axes a = 6 mm and b = 0.8 mr.)

The horizontal beamline fan is illustrated in Figure 11, where the source is represented as a point on the left and the various restrictions and masks are shown along the beamline. The transverse scale is exaggerated to show

(3) Normal operational variation in position is $\pm$ 3.0 mm horizontally and $\pm$ 1.0 mm vertically. The vertical betatron angle is less than 0.05 mr.

BML VIII BEAM ALLOTMENT

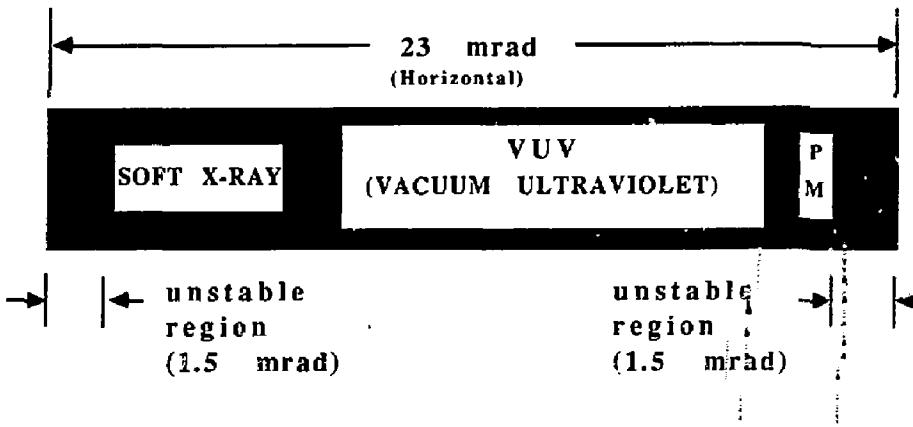

	Horizontal		Vertical
SOFT X-RAY: (60 - 1100 ev)	5.0 mrad	x	1.5 mrad
V U V : (8 - 185 ev)	12.0 mrad	x	3.0 mrad
POSITION MONTIOR :	0.7 mrad	x	1.5 mrad

Figure 10. BML VIII BEAM ALLOTMENT

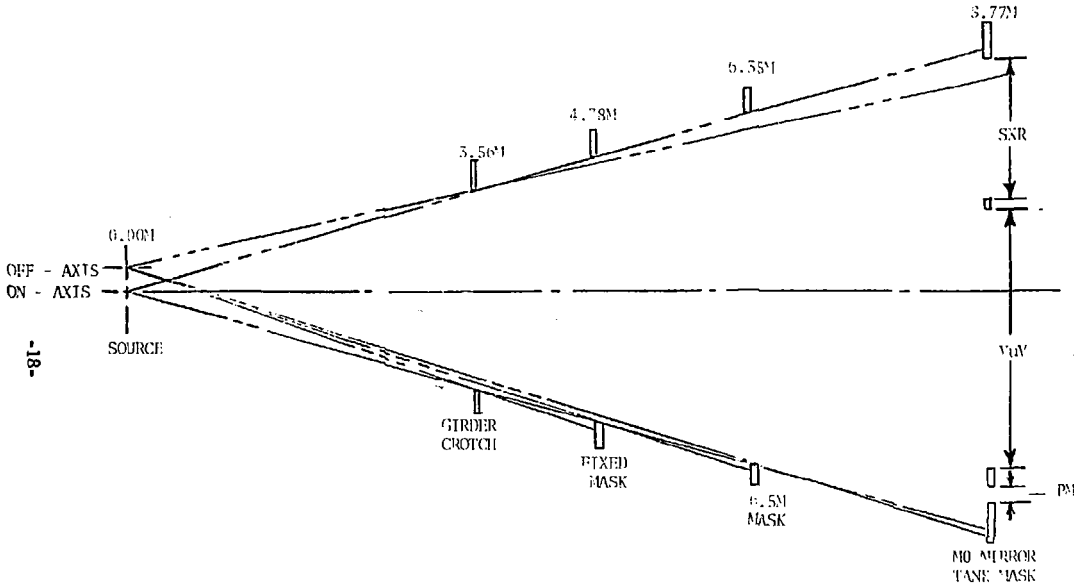

FIGURE 11. PLAN VIEW OF BEAM FAN SHOWING BEAM CUT-OFF BY VARIOUS MASKS AND RESTRICTIONS.

the restrictions more clearly. Also shown in the figure is the worst case horizontal offset of the source.

In the normal operating mode, the girder crotch restriction cast a shadow on the edges of the fixed mask at 4.78 meters and this mask in turn shadows edges of the 6.5 meter mask and the edges of the M0 mirror tank mask at 8.765 meters. When the source is offset from its reference point, the shadows are also displaced. In the worst case horizontal offset, the photon beam hits the mask in areas that are normally protected by shadows. This changes the heat loading on the masks. The fixed mask at 4.78 meters and the 6.5 meters mask have an increase in heat load as a result of a horizontal offset of the electron orbit. The heat load on the M0 mirror tank mask decreases slightly when the source point is displaced horizontally.

Vertical steering errors which change the vertical position of the electron orbit in the storage ring may produce a combination of a vertical offset and a vertical angular error in the photon beam. This error at the source may be represented by an ellipse in vertical phase space. At the source, the light rays have (y, y') coordinates. As the rays travel down the beamline toward the various mirrors, their y coordinates change but their y' values do not. The new y (y_n) value is found from

$$y_n = y + Ly'$$

where L is the drift distance.

Applying this equation to various points in the phase ellipse shows that the greatest vertical offset at the M0 mirror tank mask (L = 8765mm) occurs for the ray with source coordinates y = 3.9 mm and y' = .608 mr. For this displacement, almost all of the photon energy allocated to the SXR and PM

lines is deposited on the MO mirror tank mask as heat. There is only a negligible change in the heat deposited on the girder crotch, fixed mask, and 6.5 meter mask as a result of any expected vertical steering errors.

The results of various calculations of heat loading and energy transmission through the various masks and restrictions are summarized in Table 2. Two electron energy conditions are shown, and for each of these, the normal orbit position and the worst case source offset positions are given.

The worst case heat load on the MO mirror tank mask occurs when the MO mirror is retracted.

TABLE 2 THERMAL LOADS ON MASKS

Condition	A	B
Electron Energy, GeV	3.0	3.7
Current, mA	200.	100.
Radiation Power, W/mr	17.96	20.78
Girder Crotch		
Opening Angle, mr	23.6	23.6
Transmitted Power, W	423.9	490.4
Fixed Mask (4.78 m)		
Opening Angle, mr	23.1	23.1
Transmitted Power, W	414.9	480.0
Heat Absorbed(on-axis beam), W	9.0	10.4
Heat Absorbed(off-axis beam), W	17.0	19.7
Movable Mask		
Heat Absorbed, W	414.9	480.0
6.5 Meter Mask		
Opening Angle, mr	23.1	23.1
Transmitted Power, W	414.9	480.0
Heat Absorbed(on-axis beam), W	0.	0.
Heat Absorbed(off-axis beam), W	9.6	11.1
M0 Mirror Mask		
Opening Angle, mr	12.36	12.36
Transmitted Power, W	222.0	256.8
Intercept Angle, mr	1.18	1.18
Heat Absorbed, W	21.2	24.6
M0 Mirror Tank Mask		
Opening Angle for SXR, mr	5.76	5.76
Transmitted Power, W	103.4	119.7
Opening Angle for FM, mr	.725	.725
Transmitted Power, W	13.0	15.1
Heat Absorbed(on-axis beam), W	55.2	63.8
Heat Absorbed(horiz. displ.), W	36.8	42.5
Heat Absorbed(vert. displ.), W	159.7	184.7
Heat Absorbed(M0 retracted), W	403.0	471.2
VUV line		
M0 Mirror Incident Power, W	243.3	281.4
SXR line		
'M0' Mirror Incident Power, W	103.4	119.7
FM line		
Incident Power, W	13.0	15.1

HEAT LOADS ON MIRRORS

The masks act to shadow the edges of mirrors and all uncooled components to reduce the stray reflected light. As such, the masks also act to limit the portion of the energy striking the surface of the mirrors. Only a small percent of the energy falling upon the first mirrors is reflected; while a large percent is absorbed as heat. The amount reflected is, of course, dependent upon the reflectivity of the mirror surface. This reflectivity is shown for the platinum surface coating in Figure 12. Clearly, the reflectivity is a function of photon energy (wavelength) and of the angle of incidence. An angle can be selected to give a "fall off" in reflectivity above a particular value of photon energy.

For the VUV line, an angle of incidence of 6 degrees (100 mr) was selected to give a significant cutoff above 200 eV. For the SXR line, an angle of incidence of 2.5 degrees (44 mr) was selected to give a large drop in refectivity above 1.5 keV.

Combining the reflectivity characteristic and the spectral power distribution, a curve of reflected power vs photon energy can be obtained. Integrating this curve gives the total power reflected from the mirror. The difference between the incident and reflected power gives the heat input to the mirror. Figures 13, 14, 15, and 16 show the integrated percent of power reflected as a function of energy for the first mirrors of the VUV and SXR lines at two different electron energy levels. The shallow angle (2.5°) SXR reflects a much higher percent of the incident energy as would be expected. Increasing the electron beam energy from 3.0 GeV to 3.7 GeV decreases the percent of power reflected because of the changes in the radiation spectrum gives much more high energy (short wavelength) radiation. This high energy radiation is not reflected.

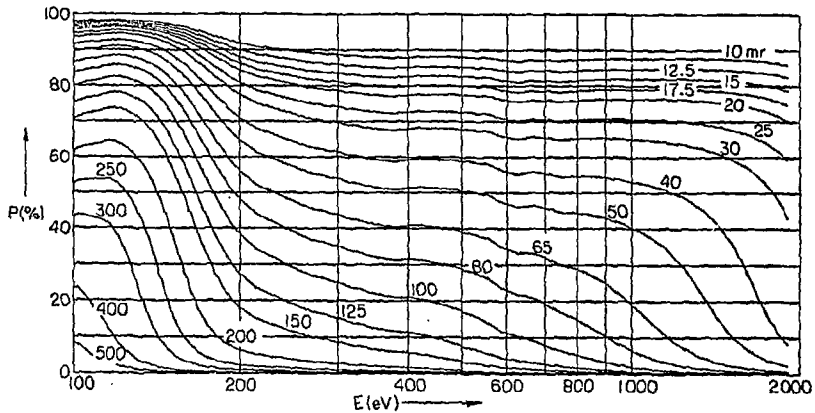

FIGURE 12. REFLECTIVITY OF PLATINUM

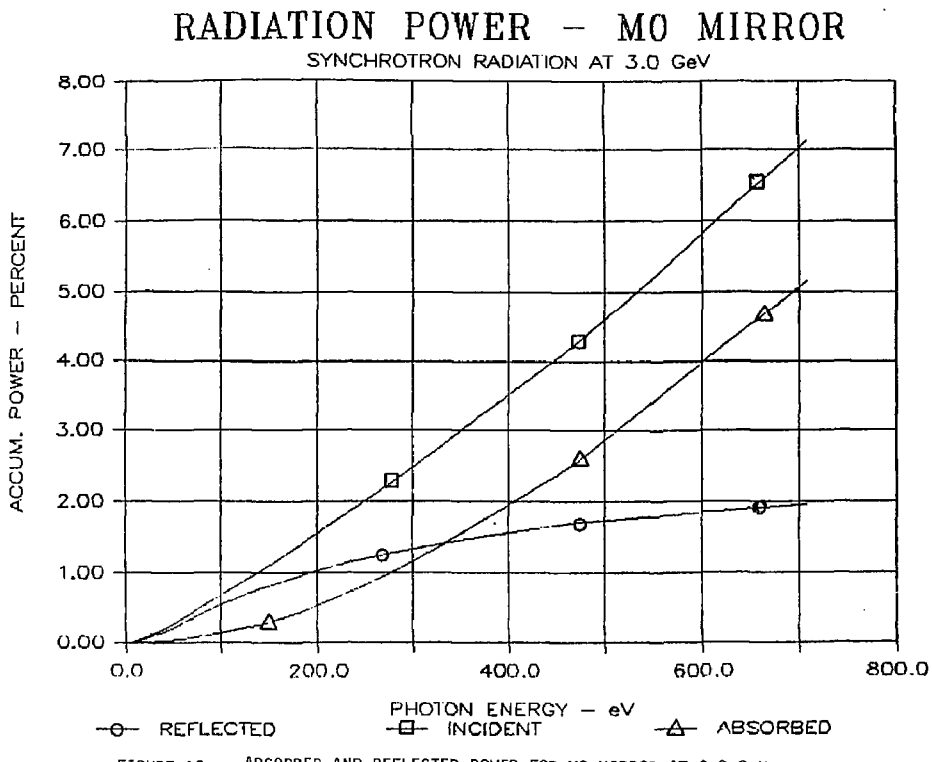

FIGURE 13. ABSORBED AND REFLECTED POWER FOR MO MIRROR AT 3.0 GeV.

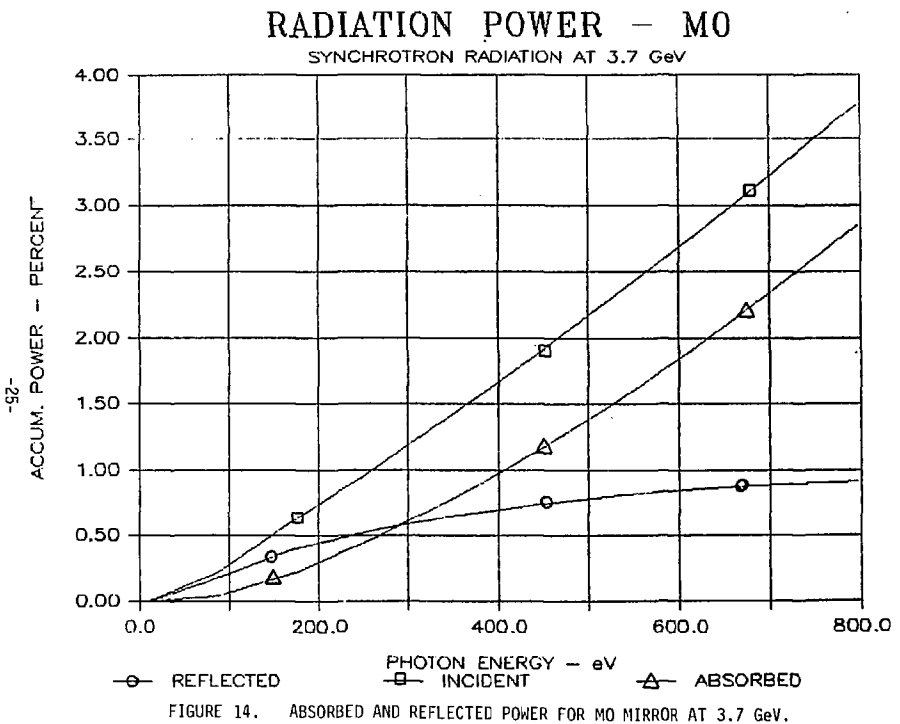

FIGURE 14. ABSORBED AND REFLECTED POWER FOR MO MIRROR AT 3.7 GeV.

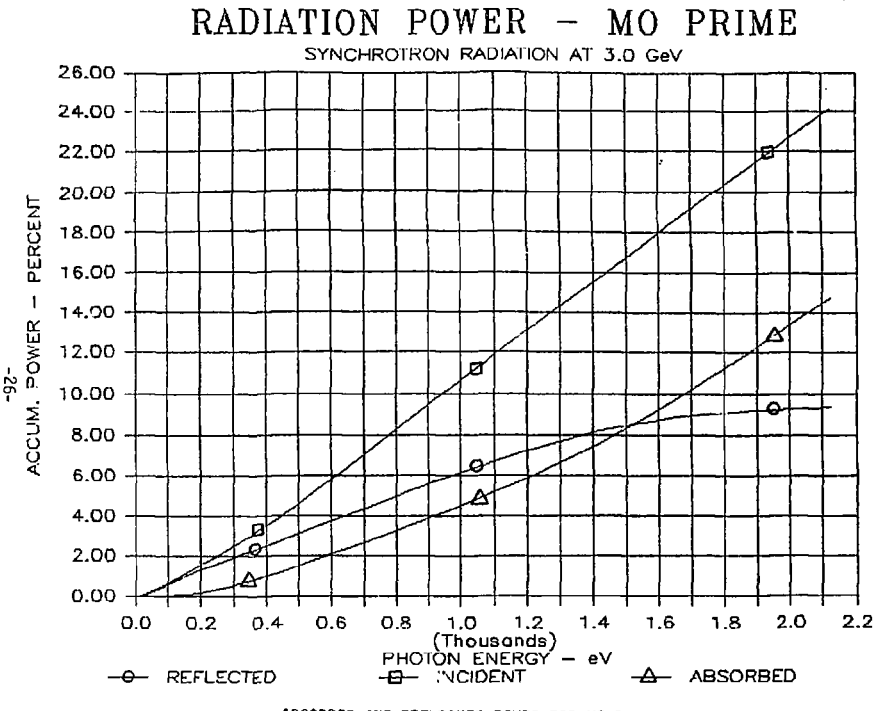

FIGURE 15. ABSORBED AND REFLECTED POWER FOR MO PRIME MIRROR AT 3.0 GeV.

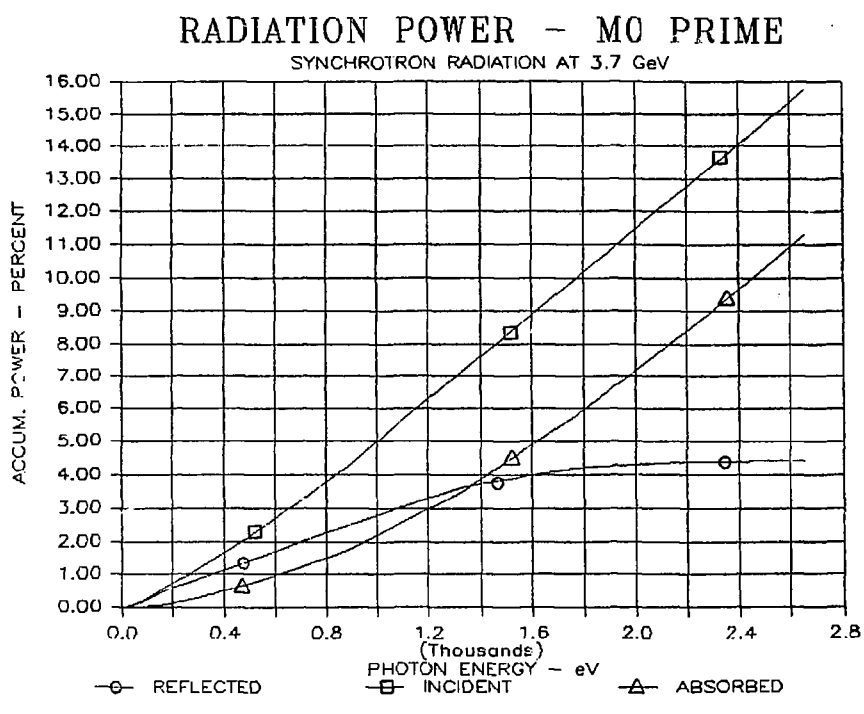

FIGURE 16. ABSORBED AND REFLECTED POWER FOR MO PRIME MIRROR AT 3.7 GeV.

The second mirror (M1) in the VUV line has the same reflectivity and angle of incidence as the first mirror. However, most of the photon striking this mirror are at low energy due to the filtering action of the first mirror. As a result, a larger percent of the light striking this mirror is reflected. The M1 mirror acts as a second filter and has the effect of sharpening the energy cutoff.

Figure 17 shows the accumulated reflected power vs energy for the M1 mirror. It can be noted that about 75% of the reflected power is in the spectral range of interest (8 to 185 eV).

The total power incident, reflected, and absorbed on the M0, M1, and M0-prime mirror is summarized in Table 3. The longitudinal distribution of this energy on the first mirrors (M0 and M0-prime) can be easily deduced from values previously shown in Figures 6 and 7. A good approximation for the longitudinal distribution on M1 can be obtained by using the curve for 188 eV (Figure 8).

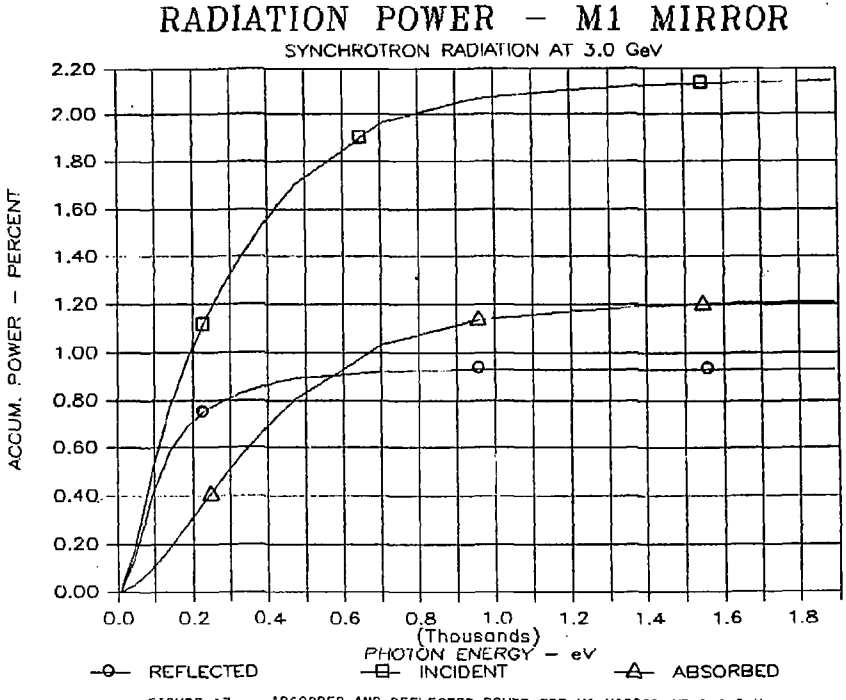

FIGURE 17. ABSORBED AND REFLECTED POWER FOR M1 MIRROR AT 3.0 GeV.

TABLE 3 HEAT LOADS ON MIRRORS

Condition	A	B
Electron Energy, GeV	3.0	3.7
Current, mA	200.	100.
Radiation Power, W/mr	17.96	20.78
Mirror M0		
Incident Energy, W	222.0	256.8
Reflected Energy, percent	2.1	.90
Reflected Energy, W	4.66	2.31
Heat Absorbed, W	217.3	254.5
Mirror M0-prime		
Incident Energy, W	103.4	119.7
Reflected Energy, percent	9.0	4.5
Reflected Energy, W	9.3	5.4
Heat Absorbed, W	94.1	114.3
Mirror M1		
Incident Energy, W	4.66	2.31
Reflected Energy, percent	43.4	40.2
Reflected Energy, W	2.02	0.93
Heat Absorbed, W	2.63	1.38
Toroidal Grating (VUV)		
Incident Energy, W	< 2.0	< .9
Reflected Energy, percent	60.	60.
Heat Absorbed, W	< 1.2	< .6
Mirror M2		
Incident Energy, W	< 1.2	< .6
Reflected Energy, percent	90.	90.
Heat Absorbed, W	< .2	< .1
SGM (SXR)		
Incident Energy, W	9.3	5.4
Reflected Energy, percent	60.	60.
Heat Absorbed, W	< 4.	< 2.5
Mirror M2-prime		
Incident Energy, W	< 6.	< 4.
Reflected Energy, percent	> 80.	> 60.
Heat Absorbed, W	< 1.5	< .8

HEAT TRANSFER REQUIREMENTS

The total amount of heat to be removed from any element is not very great, but the local heat density can be fairly high where the beam strikes normal to the surface. For example, at the edges of the fixed mask, the worst case heat load is only 19.7W, but 50% of this heat is deposited in a region 3.4 mm wide by 0.55 mm high. This gives a local heat flux of 522 W/cm^2 at the edge of the fixed mask.* A material with a good thermal conductivity is needed to aid in the removal of this heat by water flowing in cooling channels.

Because the heat transfer areas in the water cooling passages in the various elements are quite small, high heat transfer coefficients or large temperature differentials are required to obtain the desired heat transfer rates. To achieve the high heat transfer coefficients, large Reynolds number (Re) in the range from 2300 to 18000 are needed. The temperature rise in the water at the required flow rates is less than 10°F. The pressure drops associated with these high Reynolds numbers are very small (less than one psi) because the flow passages are very short.

Table 4 summarizes the required flow rates, Reynolds numbers, and heat transfer coefficients for an assumed temperature differential between the water and the wall of 10°F. The values are based on thermal and kinematic properties of water at 70°F. Most of the flow and thermal factors are computed on the assumption of turbulent flow, i.e. Re greater than 2100. As can be seen in the Table, several elements with low heat input have low Re which would indicate laminar flow. For these elements, laminar flow equations were used to calculate heat transfer coefficients and flow friction factors.

* To put a heat flux of 522 W/cm^2 in perspective, a black-body radiator with this heat flux would be at 3100°K. This is approximately the temperature of a tungsten filament.

TABLE 4.

MINIMUM COOLING WATER REQUIREMENTS FOR BEAMLINE VIII WORST CASE HEAT LOADS

COOLANT PROPERTIES VISC.= 0.010 k= 0.350 DEL T= 10.00 Pr = 6.85

ELEMENTS IN BEAMLINE	HEAT INPUT WATTS	WATER FLOW GPM	COOLING TUBE DIA. IN.	FLOW Re No. NON-DIM	HEAT TRANS. COEF.	TUBE LENGTH REQ. IN	FRIC. FACTOR NON-DIM	PRES. DROP PSI	TEMP. RISE DEG F
FIXED MASK	19.7	0.0270	0.430	198.4	71.70	10.00	0.0806	0.00018	4.982
MOVABLE MASK *	490.4	3.0000	0.277	17111.9	1937.72	2.86	0.0069	0.12851	1.116
3.5 METER MASK	11.1	0.0100	0.430	73.5	48.46	8.33	0.2177	0.00008	7.580
BEAMSTOPPER A	0.0	0.0000	0.000	0.0	0.00	0.00	0.0000	0.00000	0.000
BEAMSTOPPER B	0.0	0.0000	0.000	0.0	0.00	0.00	0.0000	0.00000	0.000
MO MIRROR & MASK1	181.4	0.6500	0.125	2067.9	1028.68	3.86	0.0112	0.08460	1.906
MO MIRROR & MASK2	100.0	0.0800	0.125	141.2	154.60	5.66	0.1133	0.00436	8.536
MIRROR TANK MASK	471.3	2.5000	0.430	18372.1	1321.27	12.98	0.0068	0.17624	1.287
MO' MIRROR & MASK	114.3	0.3790	0.277	4323.6	644.66	10.01	0.0100	0.04730	2.059
SHUTTER VUV	4.7	0.0040	0.277	45.6	87.98	3.02	0.3506	0.00005	8.024
SXR MASK	119.7	0.3000	0.404	2346.5	271.08	17.10	0.0118	0.01065	2.725
SHUTTER SXR **	119.7	0.3000	0.277	3422.4	534.71	12.64	0.0106	0.00790	2.725
SXR BEAMSTOPPER	119.7	0.3500	0.400	2765.0	312.20	15.00	0.0113	0.00970	2.335
IM BEAMSTOPPER	15.1	0.1500	0.170	2788.2	739.51	1.88	0.0113	0.01602	0.687

* MOVABLE MASK USES TWO PARALLEL PATHS AND NEEDS A TEMP DIFF OF 25 DEGREES FOR HEAT TRANS.
MO MIRROR & MASK1 IS THE HIGH HEAT REGION WITH FOUR PARALLEL PATHS
MO MIRROR & MASK2 IS THE LOW HEAT REGION WITH TEN PARALLEL PATHS
** SHUTTER SXR DOWNSTREAM OF MASK HAS ONLY 9.3 WATTS.

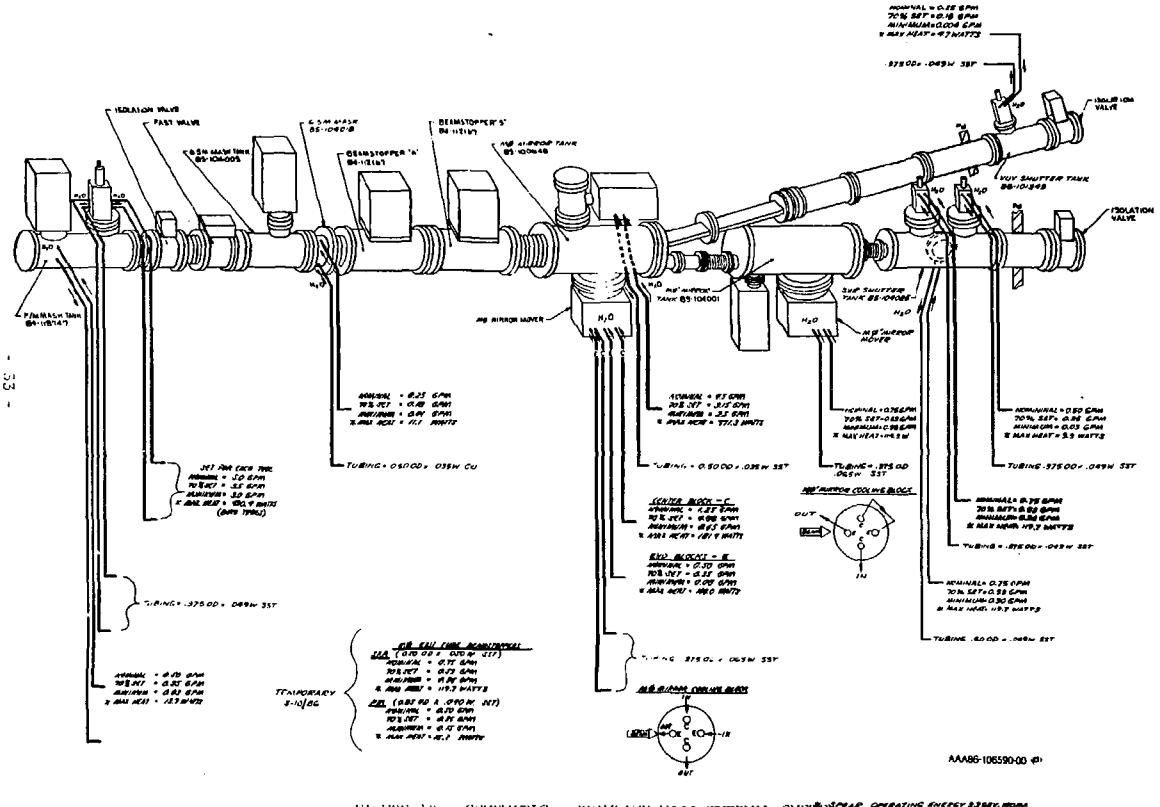

FIGURE 18. SCHEMATIC - BEAMLINE VIII THERMAL SYSTEM

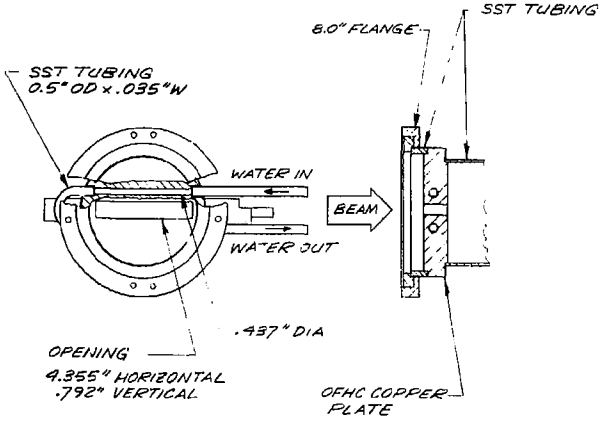

AAA86-107080-00

FIGURE 19. FIXED MASK

MOVEABLE MASK

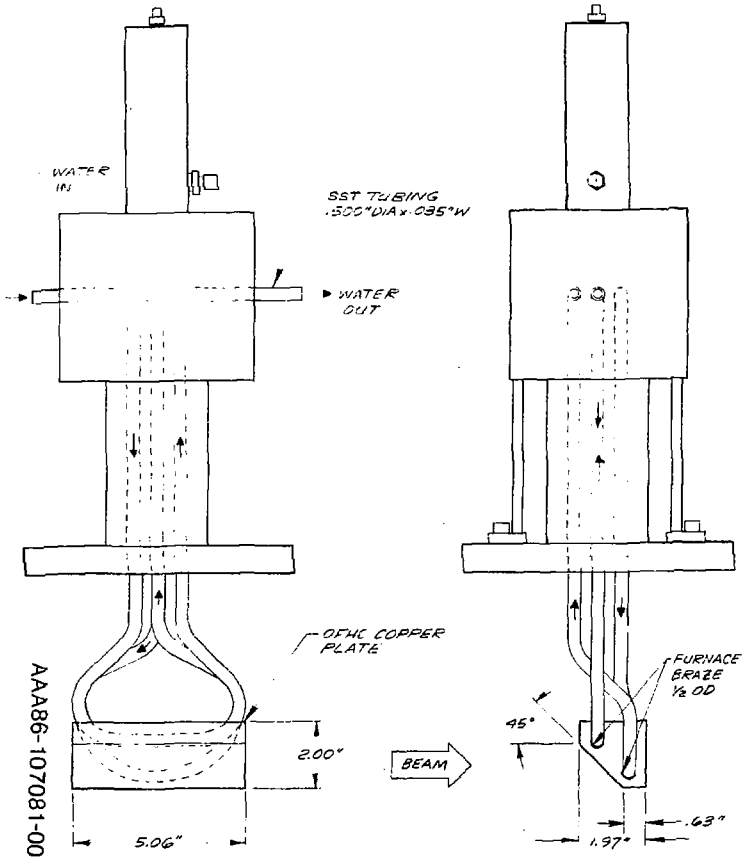

FIGURE 20. MOVEABLE MASK

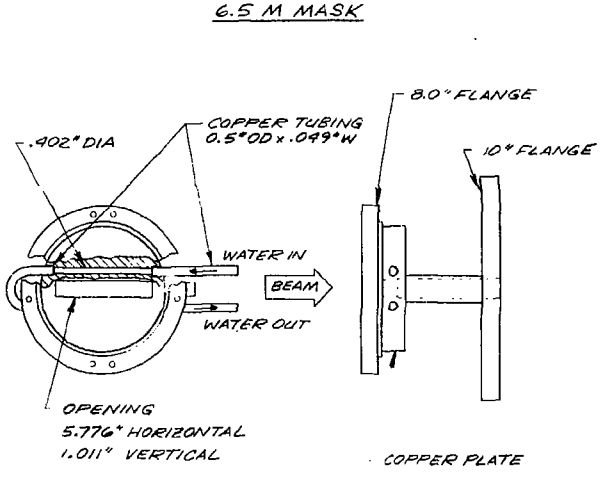

AAA86-107082-00

FIGURE 21. 6.5 M MASK

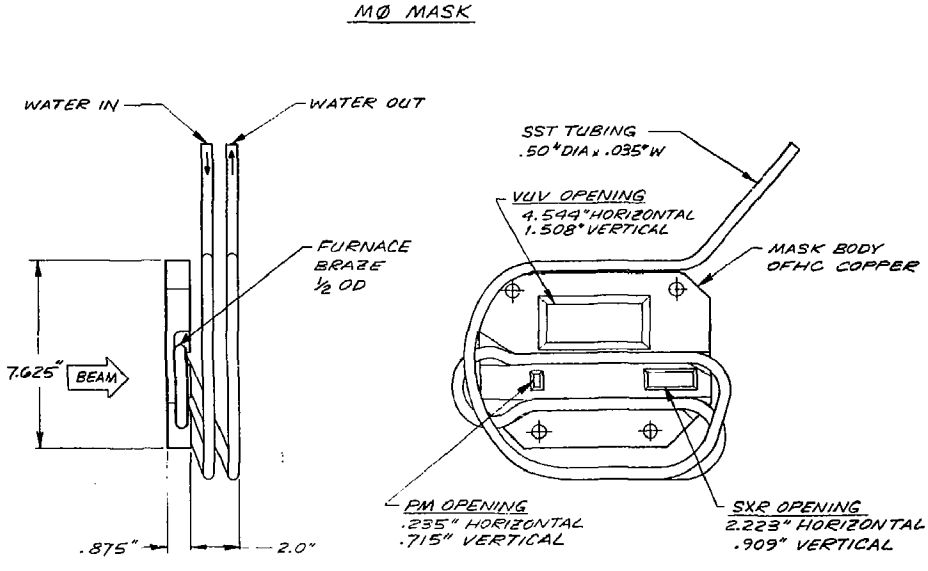

FIGURE 22. MO MIRROR TANK MASK

SXR MASK

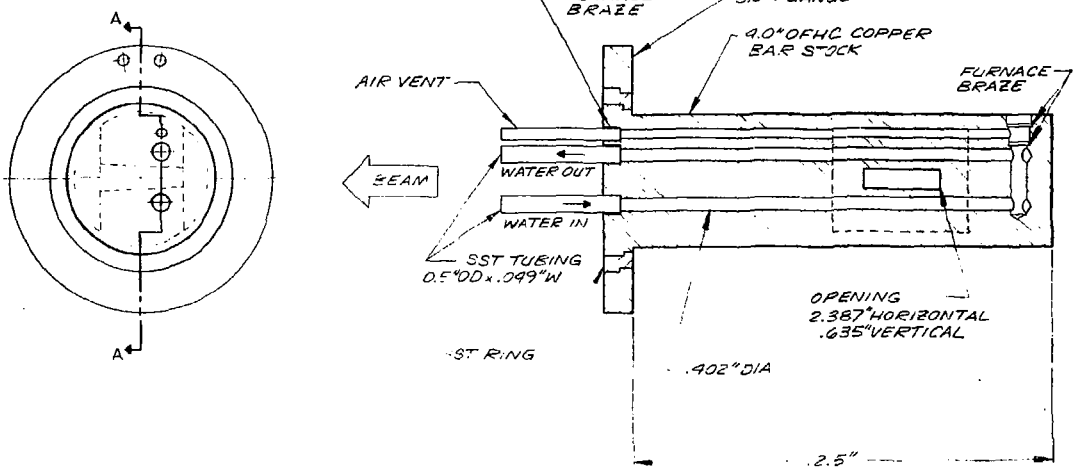

SECTION A-A

AAA86-107084-00

FIGURE 23. SXR MASK

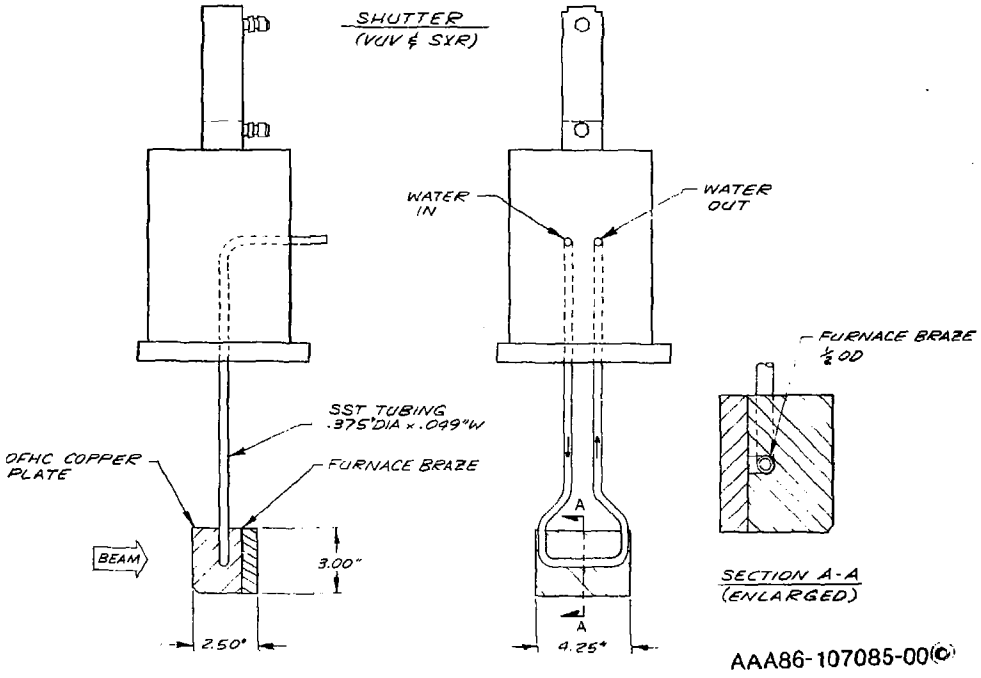

FIGURE 24. SHUTTER (VuV and S X R)

ACKNOWLEDGEMENT

The authors wish to gratefully acknowledge the review and helpful suggestions offered by Egon Hoyer, Lawrence Berkeley Laboratory.

APPENDIX I

ANALYTICAL METHODS

SYNCHROTRON RADIATION CALCULATIONS

All radiation power distributions were calculated using equations from "Properties of Synchrotron Radiation" by Herman Winick.

The total radiation power is obtained from the referenced equation #4

$$P(\mathrm{kW}) = 88.47E^4 I/\rho = 2.654BE^3 I \qquad (1)$$

Where Energy E in GeV

Current I in amperes

Radius ρ in meters

To obtain power per radian, we divide by 2π

The critical wavelength and critical energy is found from the reference equation #9

$$\lambda_c(\text{Å}) = 5.59\rho/E^3$$
$$\epsilon_c(\mathrm{keV}) = 2.218E^3/\rho \qquad (2)$$

The spectral distribution of power which were shown in Figures 2 and 3 were calculated using the reference equation #12

$$P(\lambda) = 1.421 \times 10^{-13}\frac{\gamma^2}{\rho^2} G_3(y)\frac{\mathrm{erg}}{\text{Å sec mA (mrad } \theta)}, \quad \text{for all } \psi \qquad (3)$$

Where $\gamma = E/mc^2 = 1.957 \times 10^3 E(\mathrm{GeV})$

$y = \lambda_c/\lambda = \epsilon/\epsilon_c$

$G_1(y) = y^{\frac{1}{2}} G_0(y)$

$G_0(y) = \int_y^\infty K_{5/3}(\eta)\, d\eta$

The $G_0(y)$ values are tabulated in the reference.

The accumulative power for Figures 4 and 5 are calculated by numerical intergration of the power spectrum obtained from equation #(3).

The power distributions with respect to the vertical angles shown in Figures 6 and 7 were calculated using the reference equation #10.

$$P(\psi, t) = \frac{7}{16}\frac{e^2 c}{\rho^2}\gamma^5[1 + X^2]^{-5/2}\left[1 + \frac{5}{7}\frac{X^2}{1 + X^2}\right]\frac{\text{erg}}{\text{sec rad}} \qquad (4)$$

Where $X = \gamma\psi$, and

ψ is the angle between the direction of photon emission and the instantaneous orbital plane.

The distribution curve was numerically integrated to obtain the accumulative power.

The vertical distribution at specific photon wavelengths shown in Figures 8 and 9 were calcualted using the reference equation #6.

$$P(\lambda, \psi, t) = \frac{27}{32\pi^3}\frac{e^2 c}{\rho^3}\left(\frac{\lambda_c}{\lambda}\right)^4\gamma^8(1 + X^2)^2 \times \left[K_{2/3}^2(\xi) + \frac{X^2}{1 + X^2}K_{1/3}^2(\xi)\right]\frac{\text{erg}}{\text{sec rad cm}} \qquad (5)$$

$\xi = \lambda_c[1 + X^2]^{3/2}/(2\lambda)$, and

$K_{1/3}$ and $K_{2/3}$ are modified Bessel functions of the second kind.

The value of these Bessel functions are tabulated in the reference, but for the calculations for Figures 8 and 9, it was more convenient to represent these functions by power series using relationships from "Electromagnetic Theory" by Ernst Webber. The values from the series calculation agree with the tabulated values over the range of interest.

HEAT TRANSFER CALCULATIONS

The calculation of heat transfer coefficients and flow characteristics were calculated using equations from "Heat Transmission" by W. H. McAdams, Second Edition, and "Heat and Mass Transfer," E.R.G. Eckert and R. M. Drake, 1959.

The convection heat transfer coefficients for turbulent flow (Reynolds number greater than 2100) are found from Eckert & Drake, Pg. 211.

$$Nu_d = 0.0213(Re_d)^{0.8}(Pr)^{0.4} \qquad (6)$$

Where

$Re_d = \frac{v_m d}{\nu}$ = Reynolds number - Dimensionless

$Pr = \frac{\mu c_p}{k}$ = Prandtl number - Dimensionless

$Nu_d = \frac{hd}{k}$ = Nusselt number - Dimensionless

The heat transfer coefficient for laminar flow (Reynolds number less than 2100) is found from McAdams equation 19, Pg. 190.

$$Nu_d = 1.86\left(\frac{\mu}{\mu_s}\right)^{.14}\left[(Re_d)(Pr)\left(\frac{D}{L}\right)\right]^{.33} \qquad (7)$$

Where μ is the viscosity at the average bulk temperature and μ_s is the viscosity at the average temperature of the inside surface of the tube, and D/L is the tube diameter to length ratio.

The prandtl number, viscosity, μ and the thermal conductivity, k, for water are found from tabulated values.

APPENDIX: TABLE OF VARIOUS BESSEL FUNCTIONS AND INTEGRALS [a,b]

x	$K_1(x)$	$I_1(x)$	$K_0(x)$	$E_0(x,0)$	$G_0(x)$
0.0001	10.024	4[illegible]58	6.652 + 6	6.271 + 5	973
0.001	10.715	100.20	1.5330 + 5	2.910 + 4	213.6
0.002	11.192	67[illegible]56	4.514 + 4	1.155 + 4	133.6
0.004	10.376	42.621	1.422 + 4	4.551 + 3	83.49
0.006	8.995	32.509	7.233 + 3	2.677 + 3	63.29
0.008	8.116	26.820	4.478 + 3	1.817 + 3	51.92
0.010	7.456	23.096	3.057 + 3	1.348 + 3	44.50
0.020	5.781	14.498	9.723 + 2	5.335 + 2	27.36
0.030	4.932	11.017	4.946 + 2	3.096 + 2	20.45
0.040	4.386	9.052	3.061 + 2	2.102 + 2	16.57
0.050	3.991	7.762	2.110 + 2	1.555 + 2	14.03
0.060	3.683	6.837	1.556 + 2	1.214 + 2	12.22
0.070	3.437	6.136	1.203 + 2	98.37	10.85
0.080	3.231	5.583	96.25	81.94	9.777
0.090	3.054	5.130	79.05	69.69	8.935
0.100	2.900	4.753	65.27	60.25	8.182
0.150	2.343	3.513	33.57	34.15	5.832
0.200	1.979	2.802	20.66	22.59	4.517
0.250	1.714	2.329	14.14	16.26	3.663
0.300	1.509	1.987	10.34	12.34	3.059
0.350	1.343	1.725	7.915	9.713	2.607
0.400	1.206	1.517	6.263	7.850	2.225
0.450	1.809	1.347	5.082	6.474	1.973
0.500	9.890 − 1	1.206	4.205	5.424	1.742
0.550	9.018 − 1	1.086	3.534	4.602	1.549
0.600	8.251 − 1	9.828 − 1	3.009	3.947	1.386
0.650	7.571 − 1	8.933 − 1	2.589	3.414	1.246
0.700	6.965 − 1	8.145 − 1	2.249	2.975	1.126
0.750	6.422 − 1	7.455 − 1	1.967	2.610	1.020
0.800	5.932 − 1	6.839 − 1	1.733	2.302	9.250 − 1
0.850	5.489 − 1	6.288 − 1	1.535	2.040	8.465 − 1
0.900	5.086 − 1	5.794 − 1	1.367	1.816	7.740 − 1
1.00	4.384 − 1	4.945 − 1	1.098	1.454	6.514 − 1
1.25	3.079 − 1	3.406 − 1	6.712 − 1	8.771 − 1	4.359 − 1
1.50	2.202 − 1	2.402 − 1	4.337 − 1	5.557 − 1	3.004 − 1
1.75	1.594 − 1	1.722 − 1	2.906 − 1	3.642 − 1	2.113 − 1
2.00	1.165 − 1	1.248 − 1	1.998 − 1	2.445 − 1	1.508 − 1
2.25	8.581 − 2	9.132 − 2	1.399 − 1	1.672 − 1	1.089 − 1
2.50	6.354 − 2	6.726 − 2	9.941 − 2	1.160 − 1	7.926 − 2
2.75	4.727 − 2	4.981 − 2	7.142 − 2	8.145 − 2	5.811 − 2
3.00	3.531 − 2	3.706 − 2	5.178 − 2	5.772 − 2	4.286 − 2
3.25	2.645 − 2	2.767 − 2	3.781 − 2	4.123 − 2	3.175 − 2
3.50	1.988 − 2	2.073 − 2	2.778 − 2	2.964 − 2	2.362 − 2
3.75	1.497 − 2	1.558 − 2	2.051 − 2	2.144 − 2	1.764 − 2
4.00	1.130 − 2	1.173 − 2	1.521 − 2	1.558 − 2	1.321 − 2
4.25	8.545 − 3	8.853 − 3	1.132 − 2	1.138 − 2	9.915 − 3
4.50	6.472 − 3	6.693 − 3	8.455 − 3	8.338 − 3	7.461 − 3
4.75	4.909 − 4	5.059 − 3	6.332 − 3	6.132 − 3	5.626 − 3
5.00	3.729 − 3	3.834 − 3	4.754 − 3	4.523 − 3	4.250 − 3
5.50	2.159 − 3	2.220 − 3	2.697 − 3	2.481 − 3	2.436 − 3
6.00	1.255 − 3	1.287 − 3	1.541 − 3	1.373 − 3	1.404 − 3
6.50	7.317 − 4	7.495 − 4	8.855 − 4	7.659 − 4	8.131 − 4
7.00	4.280 − 4	4.376 − 4	5.113 − 4	4.299 − 4	3.842 − 4
7.50	2.509 − 4	2.562 − 4	2.965 − 4	2.426 − 4	2.755 − 4
8.00	1.474 − 4	1.504 − 4	1.725 − 4	1.376 − 4	1.611 − 4
8.50	8.679 − 5	8.842 − 5	1.007 − 4	7.837 − 5	9.439 − 5
9.00	5.118 − 5	5.209 − 5	5.890 − 5	4.480 − 5	5.543 − 5
9.50	3.023 − 5	3.073 − 5	3.454 − 5	2.569 − 5	3.262 − 5
10.00	1.787 − 5	1.816 − 5	2.030 − 5	1.478 − 5	1.922 − 5

[a] G. K. Green, BNL Report 50522, 90 pp. (1977); BNL Report 50595, Vol. II (1977).

[b] The positive or negative number following the numerical value represents powers of ten (e.g. 6.652 + 6 represents 6.652×10^6).

DISCLAIMER

This document was prepared as an account of work sponsored by an agency of the United States Government. Neither the United States Government nor the University of California nor any of their employees, makes any warranty, express or implied, or assumes any legal liability or responsibility for the accuracy, completeness, or usefulness of any information, apparatus, product, or process disclosed, or represents that its use would not infringe privately owned rights. Reference herein to any specific commercial products, process, or service by trade name, trademark, manufacturer, or otherwise, does not necessarily constitute or imply its endorsement, recommendation, or favoring by the United States Government or the University of California. The views and opinions of authors expressed herein do not necessarily state or reflect those of the United States Government or the University of California, and shall not be used for advertising or product endorsement purposes.

Printed in the United States of America
Available from
National Technical Information Service
U.S. Department of Commerce
5285 Port Royal Road
Springfield, VA 22161

Price Code	Page Range
A01	Microfiche
Papercopy Prices	
A02	001 - 050
A03	051 - 100
A04	101 - 200
A05	201 - 300
A06	301 - 400
A07	401 - 500
A08	501 - 600
A09	601